© 2019. Published by The Company of Biologists Ltd | Journal of Cell Science (2019) 132, jcs224568. doi:10.1242/jcs.224568

RESEARCH ARTICLE

Drosophila Ptp4E regulates vesicular packaging for monoamine-neuropeptide co-transmission

Juan Tao[1,*], Dinara Bulgari[1], Drew A. Berkhoudt[1], Michael J. Calderon[2], Simon C. Watkins[2], Hector J. Fonseca Velez[3], Nadezhda Sabeva[3], David L. Deitcher[4] and Edwin S. Levitan[1,‡]

ABSTRACT

Many neurons influence their targets through co-release of neuropeptides and small-molecule transmitters. Neuropeptides are packaged into dense-core vesicles (DCVs) in the soma and then transported to synapses, while small-molecule transmitters such as monoamines are packaged by vesicular transporters that function at synapses. These separate packaging mechanisms point to activity, by inducing co-release as the sole scaler of co-transmission. Based on screening in *Drosophila* for increased presynaptic neuropeptides, the receptor protein tyrosine phosphatase (Rptp) Ptp4E was found to post-transcriptionally regulate neuropeptide content in single DCVs at octopamine synapses. This occurs without changing neuropeptide release efficiency, transport and DCV size measured by both stimulated emission depletion super-resolution and transmission electron microscopy. Ptp4E also controls the presynaptic abundance and activity of the vesicular monoamine transporter (VMAT), which packages monoamine transmitters for synaptic release. Thus, rather than rely on altering electrical activity, the Rptp regulates packaging underlying monoamine-neuropeptide co-transmission by controlling vesicular membrane transporter and luminal neuropeptide content.

This article has an associated First Person interview with the first author of the paper.

KEY WORDS: Synaptic transmission, Secretory granules, Tyrosine phosphatase, Vesicular transport, Neuropeptide vesicles

INTRODUCTION

Many synapses feature co-transmission with small-molecule transmitters that rapidly activate ionotropic receptors and neuropeptides that activate slower-acting metabotropic receptors. Spatial spread and cessation of transmission also differ between the two transmitter classes because small-molecule transmitters are rapidly taken up or degraded at the synapse, while neuropeptides can diffuse large distances before being broken down by peptidases. Based on these properties, small molecule-neuropeptide co-transmission produces complex regulation of circuits and behavior (Nusbaum et al., 2017).

[1]Department of Pharmacology and Chemical Biology, University of Pittsburgh, Pittsburgh, PA 15261, USA. [2]Department of Cell Biology, University of Pittsburgh, Pittsburgh, PA 15261, USA. [3]Department of Neuroscience, Universidad Central del Caribe, Bayamón, Puerto Rico 00960, USA. [4]Department of Neurobiology and Behavior, Cornell University, Ithaca, NY 14853, USA.
*Present address: Department of Developmental and Cell Biology, 4361 Natural Sciences II, University of California, Irvine, Irvine, CA 92697, USA.

‡Author for correspondence (elevitan@pitt.edu)

H.J.F.V., 0000-0002-5159-0755; N.S., 0000-0002-7714-4884; E.S.L., 0000-0003-3319-1344

Received 30 August 2018; Accepted 25 February 2019

Small-molecule and neuropeptide transmitters also differ in their vesicular packaging. Neuropeptides are synthesized at the endoplasmic reticulum, condensed in the trans-Golgi network (TGN) and subsequently packaged in the soma into dense-core vesicles (DCVs, also called secretory granules), which then undergo axonal transport to synapses. In contrast, small-molecule transmitters are packaged locally at synapses by vesicular transporters. For example, monoamines, such as the invertebrate norepinephrine-like transmitter octopamine, are packaged by the vesicular monoamine transporter (VMAT). The different locations and mechanisms for packaging small molecules and neuropeptides suggest that there is independent vesicular loading for the two transmitter classes. Thus, activity-induced exocytosis is the only known control point for scaling co-transmission.

Here, *Drosophila* genetics is used to identify a mutant that remarkably increases vesicular packaging of both neuropeptides and monoamines. Specifically, the receptor protein tyrosine phosphatase (Rptp) Ptp4E is shown to control neuropeptide packaging without altering DCV size in *Drosophila* octopamine boutons. Monoamine packaging is regulated in parallel in the same boutons based on changing synaptic VMAT abundance, thus demonstrating Rptp-dependent scaling of small-molecule and neuropeptide packaging mechanisms underlying co-transmission.

RESULTS

Ptp4E regulates presynaptic neuropeptide stores in octopamine synapses

We screened phosphatase-related RNA interference (RNAi) constructs and mutants for the ability to increase GAL4-driven presynaptic GFP-tagged neuropeptide stores at the *Drosophila* larval neuromuscular junction (NMJ). Previously, this approach identified the pseudophosphatase Myopic as a regulator of neuropeptide release from type Ib boutons (Bulgari et al., 2018). While conducting this screen, we also noticed an effect of Ptp4E on the neuropeptide content of octopamine-containing type II synaptic boutons, which are readily identified by their unique morphology revealed by cell surface labeling with anti-horseradish peroxidase (HRP). The effect of Ptp4E on neuropeptide content was observed under several experimental conditions. First, fluorescence from emerald GFP-tagged *Drosophila* insulin-like peptide 2 [Dilp2 (also known as Ilp2)-GFP] (Wong et al., 2012) was induced by Tdc2-GAL4, a driver that labels octopamine neurons. In these Tdc2>Dilp2-GFP animals, the neuropeptide signal was doubled on dorsal type II boutons in the Ptp4E[1] mutant (Fig. 1A,B). Second, Dilp2-GFP in type II boutons was also increased in this mutant when neuropeptide expression was driven by the native *nSyb* promoter without GAL4 (i.e. in nSyb-Dilp2-GFP animals) (Bulgari et al., 2018), showing that the effect was not specific for the Tdc2 driver (Fig. 1C). Third, when the prohormone convertase-associated driver 386Y-GAL4 was used to express emerald GFP-tagged rat

Journal of Cell Science (2019) 132, jcs224568. doi:10.1242/jcs.224568

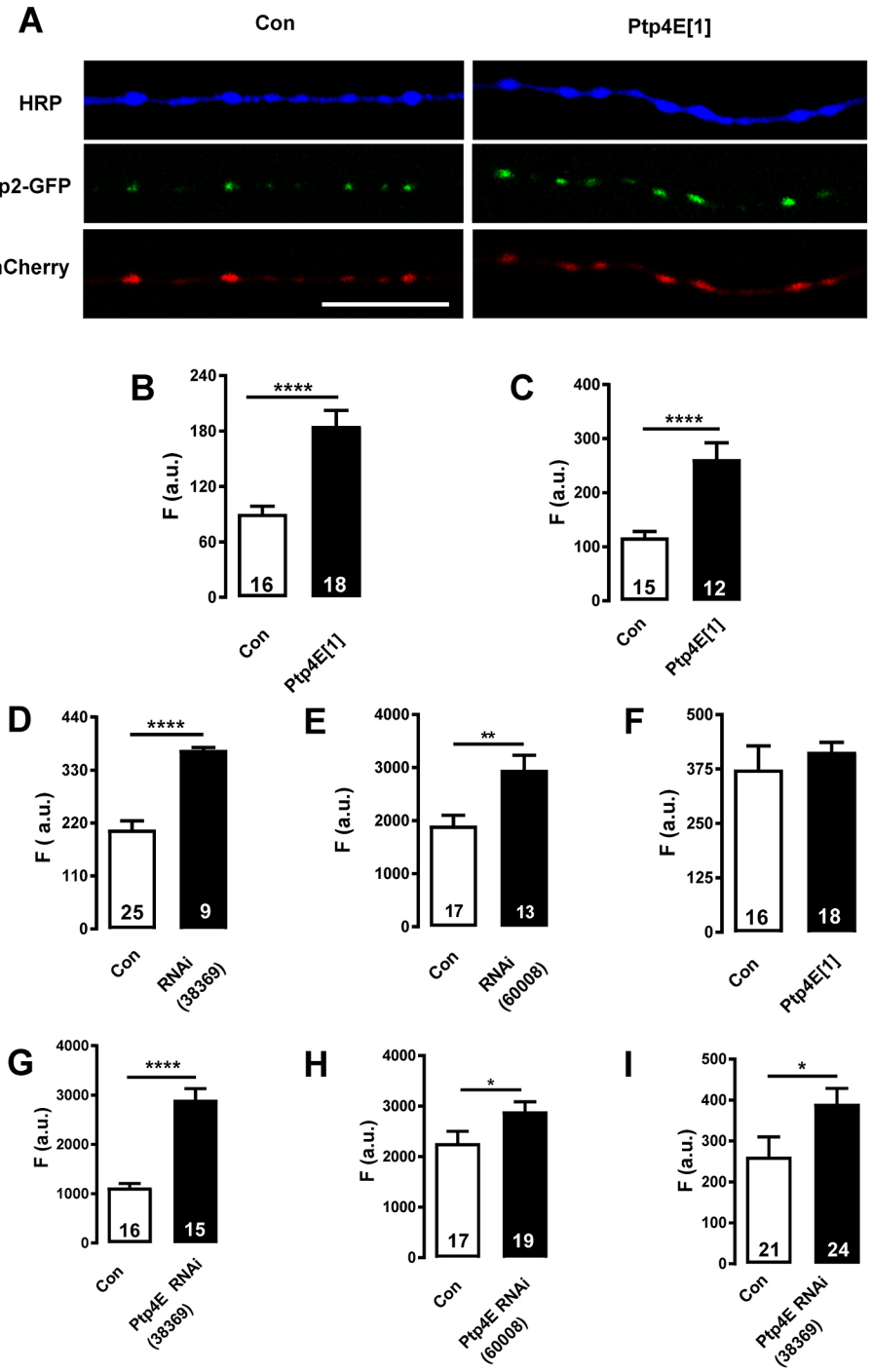

Fig. 1. Neuropeptide stores in type II boutons are increased by Ptp4E deficiency. (A) Labeling of dorsal type II boutons with HRP-Alexa Fluor 405 to label neuronal membranes, Dilp2-GFP to label DCVs and 6XmCherry to label cytoplasm. The two UAS constructs were driven by Tdc2-GAL4. Note the brighter DCV signal in the Ptp4E[1] mutant. Scale bar: 10 µm. (B) Quantification of the effect of Ptp4E[1] on Dilp2-GFP. (C) The Ptp4E[1] effect is evident when Dilp2-GFP expression is driven by the *nSyb* promoter without involvement of GAL4. (D) Effect of *Ptp4E* RNAi (BI #38369) on ANF-GFP in type II boutons driven by 386Y-GAL4. (E) Same as in D except for use of another RNAi line (BI #60008). (F) Ptp4E[1] does not affect 6XmCherry expression driven by Tdc2-GAL4. (G–I) Quantification of the effect of *Ptp4E* RNAi in Tdc2>Dilp2-GFP (G,H) and nSyb-Dilp2-GFP (I) animals. Two RNAi lines were used: BI #38369 in B, D, G and I (and all subsequent figures), and BI #60008 in C and H. Numbers of boutons analyzed are indicated in bars. Data in B–F were from 4–8 animals; data in G–I were from 5–8 animals. **P*<0.05, ***P*<0.01, *****P*<0.001. *P*-values are from two-tailed Student's *t*-test. a.u., arbitrary units; F, fluorescence.

atrial natriuretic factor [ANF (also known as Nppa)-GFP] (Han et al., 1999; Rao et al., 2001) and either of two *Ptp4E* RNAi constructs, type II bouton presynaptic neuropeptide stores increased (Fig. 1D,E), further showing that the Ptp4E effect persists with numerous drivers and neuropeptides. Finally, we examined a soluble protein to test for a global change in gene expression in octopamine neurons. In contrast to the effects on neuropeptides, the Ptp4E mutant did not affect fluorescence from soluble 6XmCherry protein in type II boutons (Fig. 1F). The differential regulation of GFP-tagged neuropeptides and a soluble protein shows that the Ptp4E mutant increases presynaptic neuropeptide stores in octopaminergic type II boutons by a post-transcriptional mechanism.

Neuron subtype selectivity of the Ptp4E effect

To address whether the Ptp4E effect is cell autonomous, the effect of targeted cell type-specific expression of RNAi constructs designed to knock down Ptp4E was determined. In these experiments, Dilp2-GFP expression was induced either by Tdc2-GAL4 (Fig. 1G,H), or independently of GAL4 with the *nSyb* promoter (Fig. 1I). In all cases tested, knockdown RNAi lines (BI #38369 and #60008) driven by Tdc2-Gal4 displayed increased type II bouton neuropeptide fluorescence (Fig. 1G–I). Therefore, the Ptp4E effect is cell autonomous.

We then considered whether Ptp4E regulation of presynaptic neuropeptide accumulation occurs in all neurons. To this end, we

Journal of Cell Science (2019) 132, jcs224568. doi:10.1242/jcs.224568

first examined GFP-tagged neuropeptides in nearby type Ib glutamatergic boutons that reside on the same postsynaptic target. Strikingly, Dilp2-GFP and ANF-GFP driven by Ok6-GAL4 and 386Y-GAL4, respectively, were not affected by *Ptp4E* RNAi (Fig. 2A–C; Bl #38369 was used here and in all subsequent RNAi figures). Likewise, the Ptp4E[1] mutant did not affect Dilp2-GFP driven by the *nSyb* promoter in peptidergic type III boutons on muscle 12 (measured at the level of whole boutons) or DCV trafficking between boutons (Fig. S1). Therefore, the presynaptic neuropeptide effect of Ptp4E is selective for type II boutons produced by octopamine neurons.

Previous studies showed that Ptp4E deficiency has little impact in embryonic glutamatergic motor neuron axon guidance and trachea because of the redundant function of the closely related gene *Ptp10D*, while dual Ptp4E, Ptp10D mutants are lethal (Jeon et al., 2008; Jeon and Zinn, 2009). These observations led us to test the hypothesis that type II boutons are dependent on Ptp4E because they lack Ptp10D. Consistent with this hypothesis, Ptp10D immunofluorescence was associated with type I boutons, but not with type II boutons (Fig. 2D). Furthermore, exogeneous expression of Ptp10D in octopamine neurons (see Materials and Methods) reversed the increase induced by Ptp4E[1] (Fig. 2E). The rescue of the mutant phenotype along with the normal absence of Ptp10D in type II boutons shows that the neuron subtype specificity for control of presynaptic neuropeptide stores by Ptp4E is produced by neuron subtype-dependent expression of Rptp family members.

Ptp4E increases vesicular neuropeptide packaging

We next examined the basis of the increase in type II bouton neuropeptide stores. First, depolarization was used to induce release, which was measured as the loss of Dilp2-GFP fluorescence. These experiments showed that Ptp4E did not affect normalized release (Fig. 3A); thus, absolute release increases in proportion to increased stores. Second, transport of DCVs was visualized between type II boutons through the cuticle of intact anesthetized larvae (Tao et al., 2017) or in fillets (Shakiryanova et al., 2006) to ensure optimal signal to noise (Fig. 3B). Genetically perturbing Ptp4E did not affect anterograde and retrograde DCV velocities and flux (Fig. 3C,D). These data suggest that the number of DCVs produced and transported to synaptic boutons does not

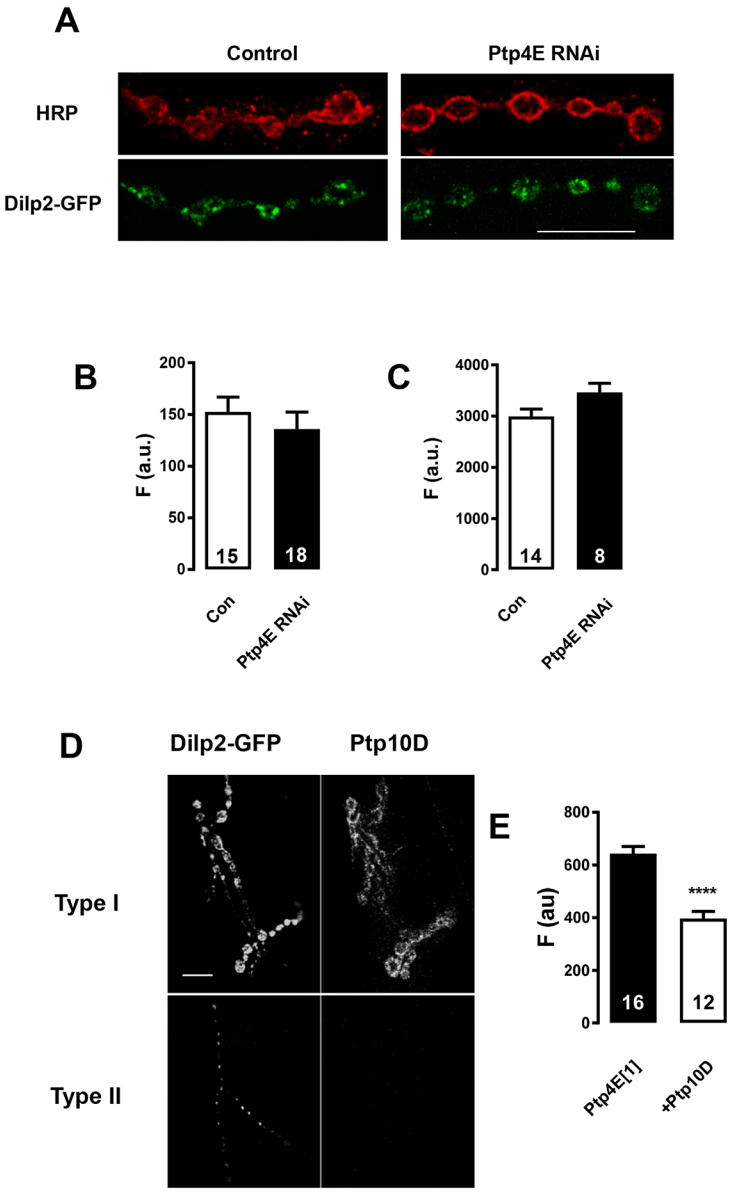

Fig. 2. Selectivity of Ptp4E regulation of neuropeptide stores and Ptp10D expression. (A) *Ptp4E* RNAi does not affect Dilp2-GFP type I boutons. Expression was driven by Ok6-GAL4. Scale bar: 10 µm. (B) Quantification of the experiment shown in A. (C) Similar to B, except that ANF-GFP was driven by 386Y-GAL4. (D) Ptp10D immunofluorescence and Dilp2-GFP in type I and II boutons of nSyb-Dilp2-GFP NMJs. Images are representative of 4 animals. Scale bar: 10 µm. (E) Ptp10D expression reverses the presynaptic neuropeptide upregulation induced by Ptp4E[1]. Numbers of boutons are indicated in bars. Data in B and C were from 5–6 animals; data in E were from 3–4 animals. ****P<0.0001, two-tailed Student's t-test.

Journal of Cell Science (2019) 132, jcs224568. doi:10.1242/jcs.224568

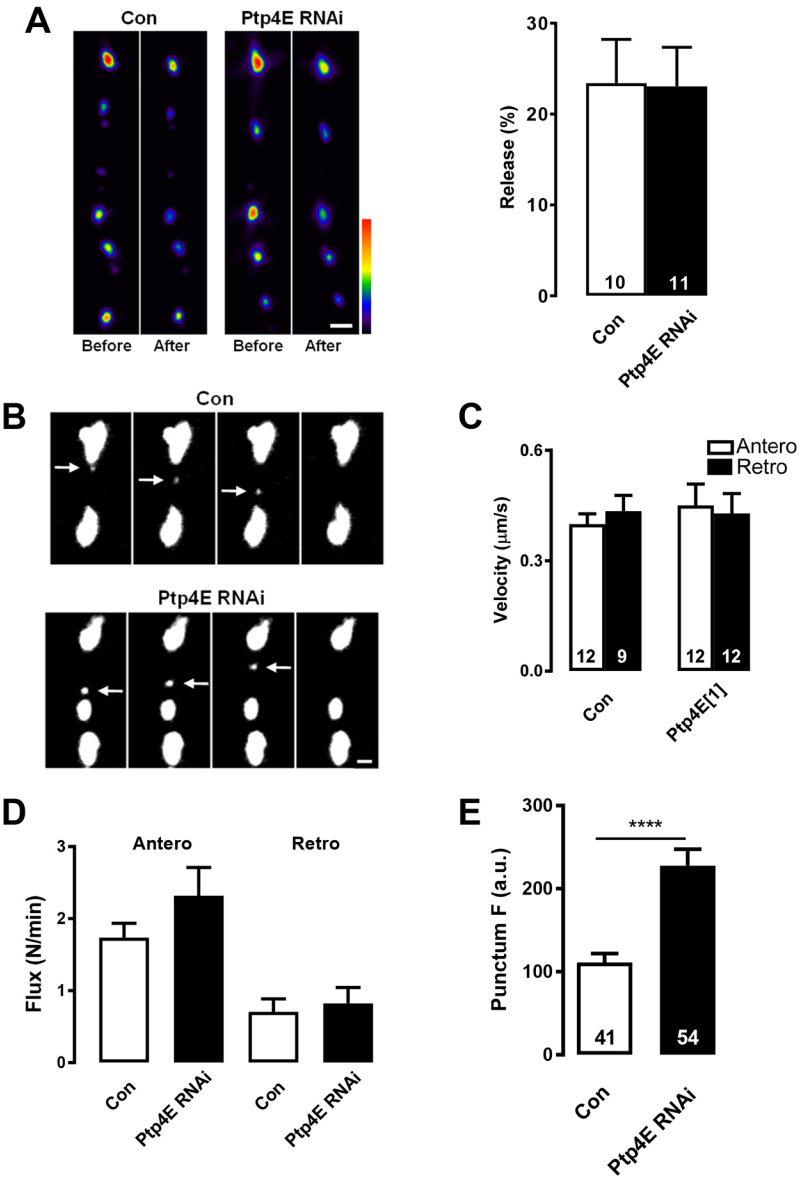

Fig. 3. Mechanism underlying Ptp4E effect on synaptic neuropeptide stores. (A) Left: pseudo-color images of boutons before and after release of Dilp2-GFP by depolarization for 3 min in control and *Ptp4E* RNAi animals. Scale bar: 2 µm. Right: quantification shows that *Ptp4E* RNAi does not affect normalized release. Numbers of boutons analyzed are indicated in bars. Data were from 3 animals for each group. (B) Time-lapse images acquired at 1 Hz show DCV puncta moving between boutons in control and *Ptp4E* RNAi filleted animals expressing Dilp2-GFP. Scale bar: 1 µm. (C) Quantification of DCV velocity in control and Ptp4E[1] intact animals. Numbers of puncta analyzed are indicated in bars. Data were from 3–4 animals. (D) DCV flux in control and *Ptp4E* RNAi intact animals. Data were from 3–6 animals. (E) Fluorescence of individual transport puncta in filleted control and *Ptp4E* RNAi animals. Numbers of puncta analyzed are indicated in bars. Data were from 3 animals for each group. ****P<0.0001, two-tailed Student's *t*-test.

account for the Ptp4E effect. Third, the number of type II boutons on muscle 2 was unchanged in the Ptp4E[1] mutant (data not shown). Finally, the brightness of transport puncta was shown to be increased with *Ptp4E* RNAi. Indeed, the observed doubling neuropeptide signal (Fig. 3E) accounts for the Ptp4E effect on type II boutons. In contrast, no increase in transport puncta signals was seen with type III (Fig. S1) or Ib boutons.

The doubling seen in type II puncta could be produced by DCVs traveling in pairs or by increasing the neuropeptide content of single DCVs. To discriminate between these possibilities, we imaged DCVs in fixed type II boutons and in the nearby interbouton axon with stimulated emission depletion (STED) super-resolution microscopy (Fig. 5A). STED microscopy showed that transport puncta detected by confocal microscopy consist of single 107±2 nm DCVs (n=38) (Fig. 4A,B). This is comparable to DCV diameter measurements in type II boutons deduced from electron microscopy (EM) (Jia et al., 1993 see below). Thus, STED microscopy accurately reported DCV size and established that DCVs are transported between boutons as individuals. STED microscopy further demonstrated that *Ptp4E* RNAi increased single-DCV GFP-neuropeptide fluorescence (Fig. 4C), thus accounting for the confocal microscopy data in living preparations (Fig. 3E). Therefore, super-resolution microscopy shows that Ptp4E deficiency increases the amount of neuropeptide packaged per individual DCV.

A potential explanation for the increased neuropeptide content could be that Ptp4E increases DCV size to accommodate more cargo. However, in contrast to this hypothesis, STED microscopy showed that the increased neuropeptide content occurred without a significant change in DCV diameter (108±2 nm versus 107±2 nm) (Fig. 4B). To independently examine whether DCV size is affected by Ptp4E without relying on expression of a GFP construct or STED microscopy, ultrastructure studies were performed on type II boutons. In accordance with a prior study (Jia et al., 1993), thin-section transmission EM revealed the presence of polymorphic DCVs (Fig. 4D). Furthermore, there was no effect of Ptp4E[1] on DCV diameter measured by EM (Fig. 4E). Therefore, super-resolution microscopy and ultrastructure experiments both show that the Ptp4E effect on DCV neuropeptide content occurs without a change in DCV size. Thus, the efficiency of neuropeptide packaging into DCVs is regulated by an Rptp.

Journal of Cell Science (2019) 132, jcs224568. doi:10.1242/jcs.224568

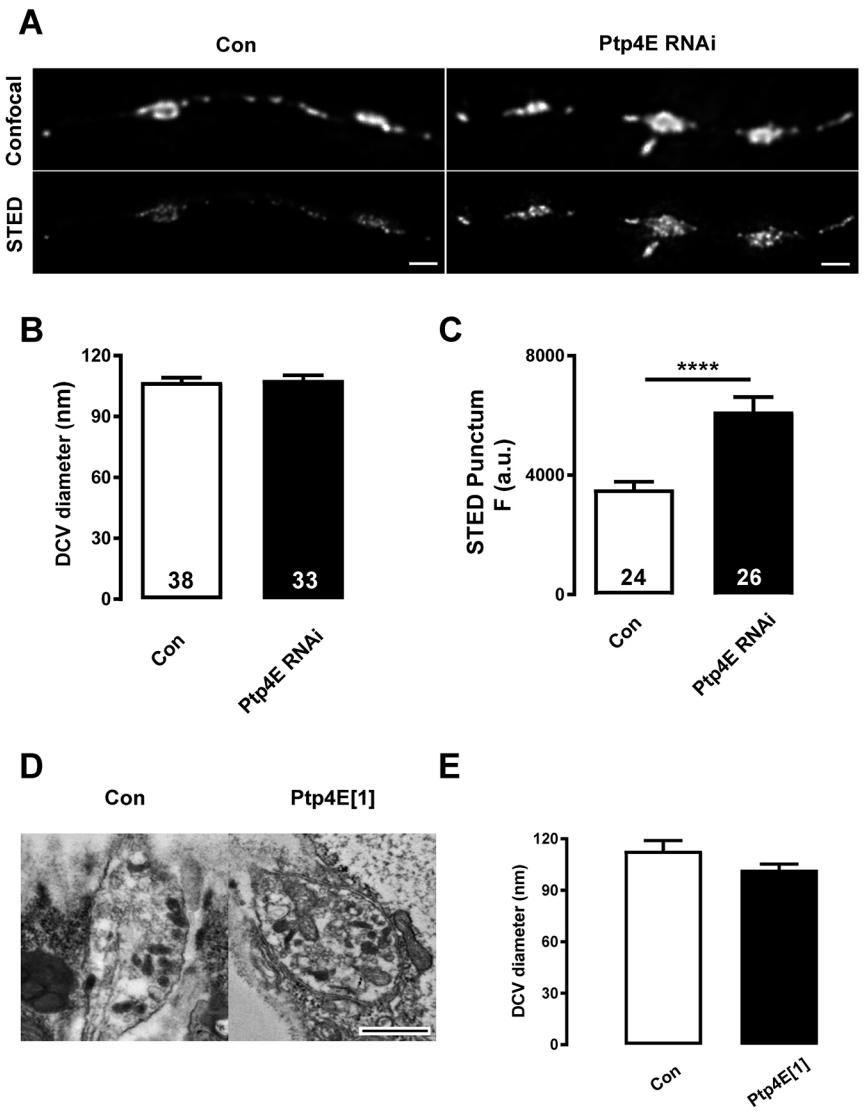

Fig. 4. Ptp4E regulates single DCV neuropeptide content without changing DCV size. (A) Confocal and STED images are shown for type II terminals in control and *Ptp4E* RNAi animals. Scale bars: 1 µm. (B,C) Quantification from STED data of diameter (B) and fluorescence (C) for puncta between boutons. Numbers of puncta are shown on each bar. Data for each measurement were from 3 animals. ****P<0.0001, from two-tailed Student's *t*-test. (D) Electron micrographs of type II boutons from control and Ptp4E[1] animals. Scale bar: 500 nm. (E) Quantification of diameter from 42 control and 76 Ptp4E[1] DCVs from 2 control and 8 Ptp4E[1] boutons.

Ptp4E regulates presynaptic VMAT expression and activity

Neuropeptides are packaged in the lumen of DCVs, while packaging of monoamines such as octopamine rely on the vesicle membrane protein VMAT. To explore whether presynaptic VMAT is affected in parallel to neuropeptide packaging, we first examined the signal from phluorin GFP-tagged VMAT (VMAT-pH) (Grygoruk et al., 2014) driven by Tdc2-GAL4. Strikingly, *Ptp4E* RNAi doubled VMAT-pH fluorescence in type II boutons (Fig. 5A, B). Given the lack of effect on Tdc2-GAL4-driven presynaptic 6XmCherry (Fig. 1E), the VMAT effect must be post-transcriptional and cell autonomous. However, because phluorin GFP is sensitive to pH, this increase could be caused by changes in protein abundance, targeting between acidic vesicles and the bouton plasma membrane or alkalinization of vesicles. To distinguish between these alternatives without the use of exogenous protein expression, native VMAT abundance in type II boutons was measured by immunofluorescence (Greer et al., 2005). Strikingly, VMAT abundance in type II boutons doubled in the Ptp4E[1] mutant (Fig. 5C,D). Because this accounts for the VMAT-pH data, an involvement of acidification is not supported. Rather, the match in the effects on the phluorin-tagged construct and the native protein, produced by a mutant or RNAi, shows that Ptp4E controls synaptic abundance of the membrane protein responsible for vesicular packaging of octopamine. Interestingly, VMAT-pH expression in type I boutons, which was induced by nSyb-GAL4, showed no sensitivity to the Ptp4E[1] mutant (P>0.4 for both type Ib and Is boutons, n=10 boutons for each measurement). Thus, as was found for luminal neuropeptide content, the effect of Ptp4E on VMAT was evident only in octopamine neurons.

To assess whether monoamine packaging is increased, we used two-photon imaging of fluorescent false neurotransmitter 206 (FFN206), which has been validated as a VMAT function indicator in *Drosophila* (Hu et al., 2013; Freyberg et al., 2016; Aguilar et al., 2017). Comparison of FFN206 accumulation in Ptp4E[1] and control animals showed that the increase in VMAT protein is associated with an increase in VMAT-mediated monoamine transport in type II boutons (Fig. 6A,B). This result is comparable to the increase in maximal capacity of isolated dopamine vesicles from transgenic mice with VMAT2 overexpression (Lohr et al., 2014). Therefore, in parallel with increased luminal neuropeptide packaging in DCVs, Ptp4E deficiency upregulates presynaptic VMAT protein to increase monoamine packaging.

DISCUSSION

Synaptic complexity is enhanced by co-transmission with small molecules and bioactive peptides. The two transmitter classes differ

Journal of Cell Science (2019) 132, jcs224568. doi:10.1242/jcs.224568

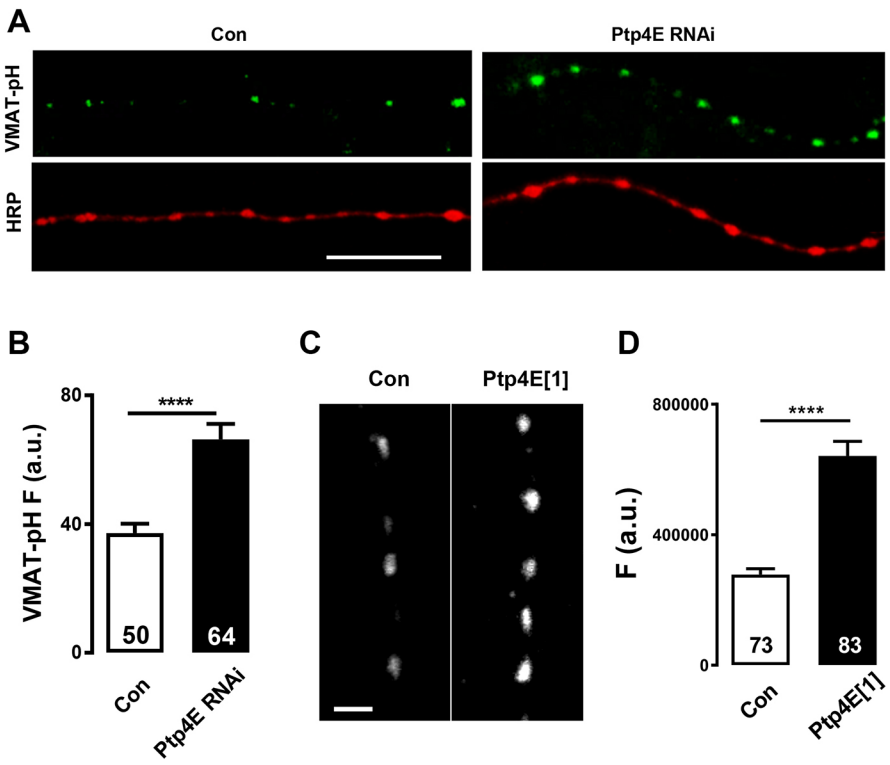

Fig. 5. Synaptic VMAT expression and activity is regulated by Ptp4E. (A) Images showing VMAT-pH driven by Tdc2-GAL4 and HRP in type II boutons of control and *Ptp4E* RNAi animals. Scale bar: 10 µM. (B) Quantification of the effect of Ptp4E on VMAT-pH fluorescence. Numbers of boutons are given in bars. Data are from 9–10 animals. (C) VMAT immunofluorescence in type II boutons of control and Ptp4E[1] animals. Scale bar: 2 µm. (D) Quantification of the effect of Ptp4E[1] on VMAT immunofluorescence based on 73 control and 83 mutant boutons studied from 3 animals of each genotype. ****P<0.0001, from two-tailed Student's t-test.

in their postrelease distances traveled and durations of action, thus providing mechanisms for rapid point-to-point control and slow neuromodulation of circuits, development and behavior. Furthermore, from a cell biology perspective, transmission by small molecules and neuropeptides is distinguished by different vesicular loading mechanisms. The genetic results presented here are remarkable because (a) they reveal increased transmitter packaging, when, to our knowledge, past genetic screens have only yielded mutants that reduce vesicular packaging; (b) control of vesicular packaging varied between neuron subtypes based on differential Rptp expression, which represents a new mechanism for generating variation in co-transmission in the nervous system. Furthermore, this result is intriguing in the context of monoaminergic neurons because Ptp4E interacts genetically with α-synuclein toxicity in *Drosophila* (Jansen et al., 2017). Given that synuclein is implicated in Parkinson's disease, DCV fusion pore dynamics and the early secretory pathway (Wang and Hay, 2015; Logan et al., 2017), the results here suggest that the mechanistic relationship between Rptps and synuclein may be broader than previously recognized; and (c) presynaptic abundance of a small-molecule vesicular membrane transporter and luminal neuropeptides are regulated in parallel. This shows that regulation of co-transmission is not limited to control of activity-induced vesicle exocytosis. Instead, an Rptp regulates vesicular packaging of both small-molecule and peptide neurotransmitters that underlies co-release.

How can a single Rptp simultaneously modify vesicular loading of both monoamines and neuropeptides? Peptidergic neurotransmission relies on packaging of neuropeptides in the soma, where they condense in the TGN and are sorted into DCVs. There is little DCV circulation in octopamine terminals because of their extensive axonal arbors and numerous boutons (Tao et al., 2017). Therefore, Rptp regulation of neuropeptide content of individual DCVs likely originates prior to axonal transport. VMAT is also processed in the TGN to be sorted into DCVs and small synaptic vesicles, rather than proceeding through the constitutive secretory pathway. A recent study found that knockdown of the TGN protein HID-1 reduces DCV luminal cargo and VMAT in DCVs by affecting sorting and DCV production (Hummer et al., 2017). The coordinated effects on neuropeptides and VMAT are reminiscent of the results here, but the Ptp4E effect on packaging was not associated with a change in DCV number or transport. Therefore, the uncoupling of DCV number from packaging is indicative of a novel cell biological mechanism. With this in mind, a possible explanation for the effect of inhibiting Ptp4E is that the tyrosine phosphorylation stimulates TGN sorting of luminal and vesicle membrane content without changing DCV number or size. By this mechanism, Rptp regulation of vesicular packaging in the soma could scale co-release at the distal synaptic ending.

Our results pose the question of the site of Ptp4E function. Rptps often mediate signaling triggered by cell–cell contacts. For example, the presynaptic Rptp Lar is activated by muscle Syndecan during development of the NMJ (Fox and Zinn, 2005; Johnson et al., 2006). By analogy, it is possible that presynaptic Ptp4E governs retrograde signaling (e.g. by interrupting tyrosine kinase-dependent mechanisms). In favor of this hypothesis, the closely related Rptp Ptp10D is found on axons in the embryo, where it is positioned to regulate axonal guidance during development (Jeon et al., 2008; Tian et al., 1991). However, the potential involvement of vesicle biogenesis (see above) and the unknown localization of Ptp4E raise the possibility that somatic Ptp4E is responsible for synaptic effects. Novel tools to differentially control of Rptp activity by compartment (i.e. soma versus terminal) will be needed to distinguish between these possibilities. Regardless of the cellular location of Ptp4E signaling, the mechanism discovered here (i.e. coincident control of packaging of neuropeptides and small-molecule transmitters) represents a previously unknown cell biological strategy for regulating synaptic co-transmission.

Previous experiments have shown that increased VMAT leads to enlargement of vesicles and greater vesicular monoamine storage

Journal of Cell Science (2019) 132, jcs224568. doi:10.1242/jcs.224568

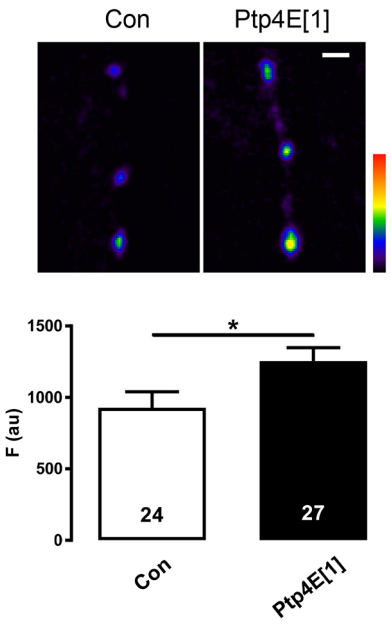

Fig. 6. Monoamine accumulation is enhanced in the Ptp4E[1] mutant. (A) Pseudo-color images showing FFN206 accumulation in type II boutons. Scale bar: 2 µM. (B) Quantification of FFN206 fluorescence in control and Ptp4E[1] boutons. Numbers of boutons are indicated in bars. Data are from 8–9 animals. *P<0.05, from two-tailed Student's t-test.

(e.g. Lohr et al., 2014), but this effect was not seen here. Notably, the mechanistic basis of the VMAT expression effect on vesicle size is not understood because thermodynamics with a simple system suggests that maximal vesicular monoamine concentration should be reached even with one VMAT per vesicle. Therefore, to explain the previously observed effect on vesicle size, some other factor, such as monoamine leakage or membrane flexibility, must come into play. We suggest that these parameters might differ in the synaptic terminals studied here. Alternatively, in contrast to the spherical vesicles studied previously, the DCVs in octopamine neurons are ovoid. Therefore, the current analysis of largest dimension cannot exclude that the narrow axis of these DCVs increased. According to the latter scenario, increases in vesicular volume and membrane surface area could have been undetected with the methodology used in the current study.

What would the expected consequences be of upregulating VMAT and neuropeptides in vesicles? Upregulating VMAT will increase the speed of vesicle loading when there is exocytosis–endocytosis cycling or kiss-and-run release. Hence, increased VMAT will affect release more when vesicle emptying by release is most marked. In *Drosophila*, the effect of increased VMAT on behavior has not been examined. However, the dopamine precursor L-DOPA increases vesicular monoamine content and ameliorates Parkinsonian symptoms in humans. Thus, by analogy, we suggest that octopaminergic signaling would be boosted by increased vesicular octopamine packaging induced by synaptic VMAT upregulation. Of course, increased co-transmission by neuropeptides could further alter octopamine action. Therefore, it would be interesting to explore how Rptps in the brain affect octopamine-dependent fly behaviors such as feeding and egg laying.

MATERIALS AND METHODS

Fly strains

UAS-ANF-GFP (UAS-preproANF-EMD), UAS-Dilp2-GFP/CyO and nSyb-Dilp2-GFP were reported previously (Bulgari et al., 2018; Wong et al., 2012; Rao et al., 2001). Tdc2>ANF-GFP and Tdc2>VMAT-pH (Grygoruk et al., 2014) were kindly provided by David Krantz (UCLA, Los Angeles, CA), while w1118 flies were provided by Zachary Freyberg (University of Pittsburgh, Pittsburgh, PA). Flies from the Bloomington *Drosophila* Stock Center include Canton S, UAS-6XmCherry (Bl #52267), UAS-*Ptp4E* RNAi (Bl #38369 and #60008), w Ptp4E[1] (Bl #42019) and w P{EP}Ptp10D^{EP1172} (Bl#11332). For studying the effect of inducing Ptp10D expression in type II boutons, w P{EP}Ptp10D^{EP1172} was crossed to w* Ptp4E[1] and the resulting w Ptp4e[1]/w P{EP}Ptp10D^{EP1172} females were crossed to FM7a males and individual w+ male progeny were selected. These males were crossed to FM7a females to generate individual stocks. Squish preps were performed on the individual male founders to determine whether the Ptp4E[1] deletion was present, using the primers 5′-TGCGA-AACCTTCGACCATCA-3′ and 5′-ATGCCAACAACAAGCCACAC-3′ to the deleted portion of Ptp4E and Q5 DNA polymerase (NEB), under manufacturer-recommended conditions. Two lines with the deletion were identified. One line was then crossed to w; Tdc2-GAL4 nSyb-Dilp2 and w; nSyb-Dilp2 to determine whether exogenous expression of PtP10D through the EP insertion and GAL4 expression could rescue the Ptp4E[1] phenotype of type II boutons.

All animals were raised at 25°C. Control crosses were based on Canton S or w1118, which produced indistinguishable results. Male RNAi flies were used for crosses and offspring of both sexes were used for data collection. For the mutant experiments, PTP4E[1] females were used in crosses and males were used for mutant data collection.

HRP, Ptp10D and VMAT immunofluorescence

For labeling neuronal membranes, live fillets were stained with anti-HRP (Jackson ImmunoResearch) antibody conjugated with either tetramethylrhodamine-isothiocyanate (TRITC; lot 120714, 1:100 dilution) or Alexa Fluor 405 (lot 124382, 1:300 dilution) for 15 min. Antibody was removed by washing 3× with Ca^{2+}-free HL3 solution for 3 min.

Ptp10D immunofluorescence was detected after treating nSyb-Dilp2-GFP fillets with Bouin's fixative for 8 min, followed by staining with Developmental Studies Hybridoma Bank (DSHB) monoclonal antibody 8B22F5 supernatant at a 1:100 dilution and then 1:1000 goat anti-mouse Alexa Fluor 568 anti-mouse antibody (Invitrogen, A11004).

For VMAT immunofluorescence, fillets were treated with Bouin's fixative for 5 min and then incubated with anti-DVMAT-A C-terminus antibody (Greer et al., 2005), kindly provided by David Krantz (UCLA), at a 1:100 dilution. Subsequently, they were treated with a secondary antibody [tetramethylrhodamine goat anti-rabbit (T2769, lot 1729638, Life Technologies, Eugene, OR)] at a 1:1000 dilution.

Imaging

All data from third-instar NMJs are on muscles 2 and 3, which are innervated by the same neuron (Hoang and Chiba, 2001). The third or fourth hemisegment from the head was examined for each animal. Filleted larvae were imaged in Ca^{2+}-free HL3 solution (70 mM NaCl, 5 mM KCl, 0.5 mM Na_3-EGTA, 20 mM $MgCl_2$, 10 mM $NaHCO_3$, 5 mM trehalose, 115 mM sucrose and 5 mM HEPES, pH 7.2). Experiments were performed on upright Olympus microscopes equipped for scanning confocal (Fluoview 1000) spinning disk (Yokogawa) confocal microscopy or two-photon microscopy (modified Fluoview 1000, see below). For fluorescent protein and HRP imaging, 20× (NA 0.95), 40× (NA 0.8 NA) or 60× (NA 1.10) dipping water immersion objectives were used with laser excitation at 405, 488 and 561 nm.

DCVs were also imaged on the confocal microscope through the cuticle in intact anesthetized larvae. Specifically, Tdc2>Dilp2-GFP larvae were exposed to isoflurane vapor for 5–7 min and then transferred to a slide with a drop of HL3 solution (i.e. same solution as above except with EGTA replaced by 1.5 mM $CaCl_2$). A coverslip (#1.5) was used to squeeze a larva flat with its dorsal side up. The slide was then viewed with a 60× (NA 1.45) oil immersion lens and to image DCVs at 0.5 Hz at a single plane of focus. If imaging was disrupted by muscle contractions, the anesthetic was applied again on the same larva for a couple of minutes or a new larva was used. A well-anesthetized larva could then be imaged for 15–20 min and fully awakened after 30–60 min of recovery on food.

Super-resolution microscopy was performed with fixed fillets. First, live fillets were stained with anti-HRP (Jackson ImmunoResearch) antibody conjugated with TRITC (lot 120714, 1:100 dilution) for 15 min, then fixed with 4% paraformaldehyde for 30 min. Then, samples were mounted in ProLong™ Diamond (Invitrogen by Thermo Fisher Scientific, lot 1804928) mounting medium with 1.5 coverslips and stored at 4°C for 5–7 days before imaging Dilp2-GFP with the Leica SP8 3× STED microscope with a 93× 1.30 NA glycerine immersion objective. Diameters were measured as full width at half maximum (FWHM).

FFN206 experiments were performed with control (w1118) and Ptp4E[1] filleted larvae in Ca^{2+}-free HL3. Cy3-conjugated anti-HRP antibody (1:400 dilution in Ca^{2+}-free HL3) was added for 20 min. After washing, type II boutons were visualized by confocal microscopy. Then, 1 µM FFN206 (Tocris Bioscience, #5043, Batch No. 1, made from a 2 mM stock solution in dimethyl sulfoxide) was added for 5 min. FFN206 was imaged with two-photon excitation at 820 nm, with a 525 nm low-pass filter on a Olympus Fluoview 1000 microscope equipped with a Coherent Chameleon Ultra laser and a nondescanned detector (LSM Technologies), with a 40× 0.8 NA water dipping objective.

Stimulation of DCV release

For stimulation of synaptic neuropeptide release, larvae expressing Dilp2-GFP were filleted in Ca^{2+}-free HL3 medium and then depolarized by application of high K^+ HL3 (i.e. same as HL3 except that 70 mM NaCl was replaced with KCl) for 3 min. Synaptic release was imaged after the medium was replaced with Ca^{2+}-free HL3 with quantification of intensity performed with ImageJ software (http://rsb.info.nih.gov/ij/), as previously described (Levitan et al., 2007). For fluorescence intensity measurements, the region of interest (ROI) in one frame was selected (e.g. containing a bouton). Then, another ROI was drawn away from boutons for background subtraction.

Transmission EM

The sample preparation protocol was used from a prior study (Sabeva and Bykhovskaia, 2017). Preparations were fixed in 4% PFA/1% glutaraldehyde in 0.2 mM $CaCl_2$ in 0.9 mM cacodylate buffer, pH 7.2–7.4, in a microwave oven (Biowave, Ted Pella) at 150 W, 25–26°C for 1 min, and incubated in the same fixative for an additional 15 min at room temperature. Samples were washed in 0.9 mM cacodylate buffer to be postfixed for 1 h in 1% osmium tetroxide while slowly rotating on PELCO® R1 Single Speed Rotator in the 35° position (Ted Pella, model PELCO® R1). Preparations were further contrasted in 2% uranyl acetate for 30–60 min and dehydrated in a graded series of 50, 70, 90 and 100% acetone. Specimens were flat embedded in Embed 812 epoxy resin using ACLAR® 33C Embedding film (Electron Microscopy Sciences, catalog number 50425-10) overnight at 60°C (oven, Binder, Tuttlingen, Germany). Preparations were serially sectioned (50 nm thick) using an ultramicrotome for ultrathin sectioning (Leica, model Leica EM UC6) and visualized using a JEOL 100 CX electron microscope equipped with AMT software. DCV diameter was determined from micrographs at 7000× magnification. To avoid duplication, every third section from the serial sectioning band of a bouton was analyzed. Micrograph analysis was performed using Adobe Photoshop CS6 (Adobe Systems) software.

Statistics

Error bars show s.e.m. Student's *t*-test and one-way ANOVA with Tukey's post-test were used to determine *P*-values in GraphPad Prism.

Acknowledgements

We thank Dr Markus Klose (University of Pittsburgh) for comments, Dr Seth Walters (University of Pittsburgh) for experimental advice, and Dr David Krantz (UCLA) for VMAT-pH flies and the anti-VMAT antibody.

Competing interests

The authors declare no competing or financial interests.

Author contributions

Conceptualization: J.T., D.L.D., E.S.L.; Methodology: J.T., D.B., D.L.D., E.S.L.; Validation: J.T., D.A.B.; Formal analysis: J.T., D.B., D.A.B., N.S., E.S.L.; Investigation: J.T., D.B., D.A.B., M.J.C., H.J.F.V., N.S.; Resources: S.C.W., N.S., D.L.D.; Writing - original draft: E.S.L.; Writing - review & editing: J.T., D.B., N.S., D.L.D.; Supervision: E.S.L.; Project administration: E.S.L.; Funding acquisition: E.S.L.

Funding

This study was supported by the National Institute of Neurological Disorders and Stroke [NS032385 to E.S.L.] and the National Institutes of Health [S10OD021540 to S.C.W.]. Deposited in PMC for release after 12 months.

Supplementary information

Supplementary information available online at
http://jcs.biologists.org/lookup/doi/10.1242/jcs.224568.supplemental

References

Aguilar, J. L., Dunn, M., Mingote, S., Karam, C. S., Farino, Z. J., Sonders, M. S., Choi, S. J., Grygoruk, A., Zhang, Y., Cela, C. et al. (2017). Neuronal depolarization drives increased dopamine synaptic vesicle loading via VGLUT. *Neuron* **95**, 1074-1088.

Bulgari, D., Jha, A., Deitcher, D. L. and Levitan, E. S. (2018). Myopic (HD-PTP, PTPN23) selectively regulates synaptic neuropeptide release. *Proc. Natl. Acad. Sci. USA* **115**, 1617-1622.

Fox, A. N. and Zinn, K. (2005). The heparan sulfate proteoglycan syndecan is an in vivo ligand for the Drosophila LAR receptor tyrosine phosphatase. *Curr. Biol.* **15**, 1701-1711.

Freyberg, Z., Sonders, M. S., Aguilar, J. I., Hiranita, T., Karam, C. S., Flores, J., Pizzo, A. B., Zhang, Y., Farino, Z. J., Chen, A. et al. (2016). Mechanisms of amphetamine action illuminated through optical monitoring of dopamine synaptic vesicles in Drosophila brain. *Nat. Commun.* **7**, 10652.

Greer, C. L., Grygoruk, A., Patton, D. E., Ley, B., Romero-Calderon, R., Chang, H.-Y., Houshyar, R., Bainton, R. J., Diantonio, A. and Krantz, D. E. (2005). A splice variant of the Drosophila vesicular monoamine transporter contains a conserved trafficking domain and functions in the storage of dopamine, serotonin, and octopamine. *J. Neurobiol.* **64**, 239-258.

Grygoruk, A., Chen, A., Martin, C. A., Lawal, H. O., Fei, H., Gutierrez, G., Biedermann, T., Najibi, R., Hadi, R., Chouhan, A. K. et al. (2014). The redistribution of Drosophila vesicular monoamine transporter mutants from synaptic vesicles to large dense-core vesicles impairs amine-dependent behaviors. *J. Neurosci.* **34**, 6924-6937.

Han, W., Ng, Y.-K., Axelrod, D. and Levitan, E. S. (1999). Neuropeptide release by efficient recruitment of diffusing cytoplasmic secretory vesicles. *Proc. Natl. Acad. Sci. USA* **96**, 14577-14582.

Hoang, B. and Chiba, A. (2001). Single-cell analysis of Drosophila larval neuromuscular synapses. *Dev. Biol.* **229**, 55-70.

Hu, G., Henke, A., Karpowicz, R. J., Sonders, M. S., Farrimond, F., Edwards, R., Sulzer, D. and Sames, D. (2013). New fluorescent substrate enables quantitative and high-throughput examination of vesicular monoamine transporter 2 (VMAT2). *ACS Chem. Biol.* **8**, 1947-1954.

Hummer, B. H., De Leeuw, N. F., Burns, C., Chen, L., Joens, M. S., Hosford, B., Fitzpatrick, J. A. J. and Martin, T. F. J. (2017). HID-1 controls formation of large dense core vesicles by influencing cargo sorting and trans-Golgi network acidification. *Mol. Biol. Cell* **28**, 3870-3880.

Jansen, I. E., Ye, H., Heetveld, S., Lechler, M. C., Michels, H., Seinstra, R. I., Lubbe, S. J., Drouet, V., Lesage, S., Majounie, E. et al. (2017). Discovery and functional prioritization of Parkinson's disease candidate genes from large-scale whole exome sequencing. *Genome Biol.* **18**, 22.

Jeon, M. and Zinn, K. (2009). Receptor tyrosine phosphatases control tracheal tube geometries through negative regulation of Egfr signaling. *Development* **136**, 3121-3129.

Jeon, M., Nguyen, H., Bahri, S. and Zinn, K. (2008). Redundancy and compensation in axon guidance: genetic analysis of the Drosophila Ptp10D/Ptp4E receptor tyrosine phosphatase subfamily. *Neural. Dev.* **3**, 3.

Jia, X.-X., Gorczyca, M. and Budnik, V. (1993). Ultrastructure of neuromuscular junctions in Drosophila: comparison of wild type and mutants with increased excitability. *J. Neurobiol.* **24**, 1025-1044.

Johnson, K. G., Tenney, A. P., Ghose, A., Duckworth, A. M., Higashi, M. E., Parfitt, K., Marcu, O., Heslip, T. R., Marsh, J. L., Schwarz, T. L. et al. (2006). The HSPGs Syndecan and Dallylike bind the receptor phosphatase LAR and exert distinct effects on synaptic development. *Neuron* **49**, 517-531.

Levitan, E. S., Lanni, F. and Shakiryanova, D. (2007). In vivo imaging of vesicle motion and release at the Drosophila neuromuscular junction. *Nat. Protoc.* **2**, 1117-1125.

Logan, T., Bendor, J., Toupin, C., Thorn, K. and Edwards, R. H. (2017). α-Synuclein promotes dilation of the exocytotic fusion pore. *Nat. Neurosci.* **20**, 681-689.

Lohr, K. M., Bernstein, A. I., Stout, K. A., Dunn, A. R., Lazo, C. R., Alter, S. P., Wang, M., Li, Y., Fan, X., Hess, E. J. et al. (2014). Increased vesicular monoamine transporter enhances dopamine release and opposes Parkinson

disease-related neurodegeneration in vivo. *Proc. Natl. Acad. Sci. USA* **111**, 9977-9982.

Nusbaum, M. P., Blitz, D. M. and Marder, E. (2017). Functional consequences of neuropeptide and small-molecule co-transmission. *Nat. Rev. Neurosci.* **18**, 389-403.

Rao, S., Lang, C., Levitan, E. S. and Deitcher, D. L. (2001). Visualization of neuropeptide expression, transport, and exocytosis in Drosophila melanogaster. *J. Neurobiol.* **49**, 159-172.

Sabeva, N. S. and Bykhovskaia, M. (2017). FM1-43 photoconversion and electron microscopy analysis at the drosophila neuromuscular junction. *Bio. Protoc.* **7**, e2523.

Shakiryanova, D., Tully, A. and Levitan, E. S. (2006). Activity-dependent synaptic capture of transiting peptidergic vesicles. *Nat. Neurosci.* **9**, 896-900.

Tao, J., Bulgari, D., Deitcher, D. L. and Levitan, E. S. (2017). Limited distal organelles and synaptic function in extensive monoaminergic innervation. *J. Cell Sci.* **130**, 2520-2529.

Tian, S. S., Tsoulfas, P. and Zinn, K. (1991). Three receptor-linked protein-tyrosine phosphatases are selectively expressed on central nervous system axons in the Drosophila embryo. *Cell* **67**, 675-685.

Wang, T. and Hay, J. C. (2015). Alpha-synuclein toxicity in the early secretory pathway: how it drives neurodegeneration in parkinsons disease. *Front. Neurosci.* **9**, 433.

Wong, M. Y., Zhou, C., Shakiryanova, D., Lloyd, T. E., Deitcher, D. L. and Levitan, E. S. (2012). Neuropeptide delivery to synapses by long-range vesicle circulation and sporadic capture. *Cell* **148**, 1029-1038.

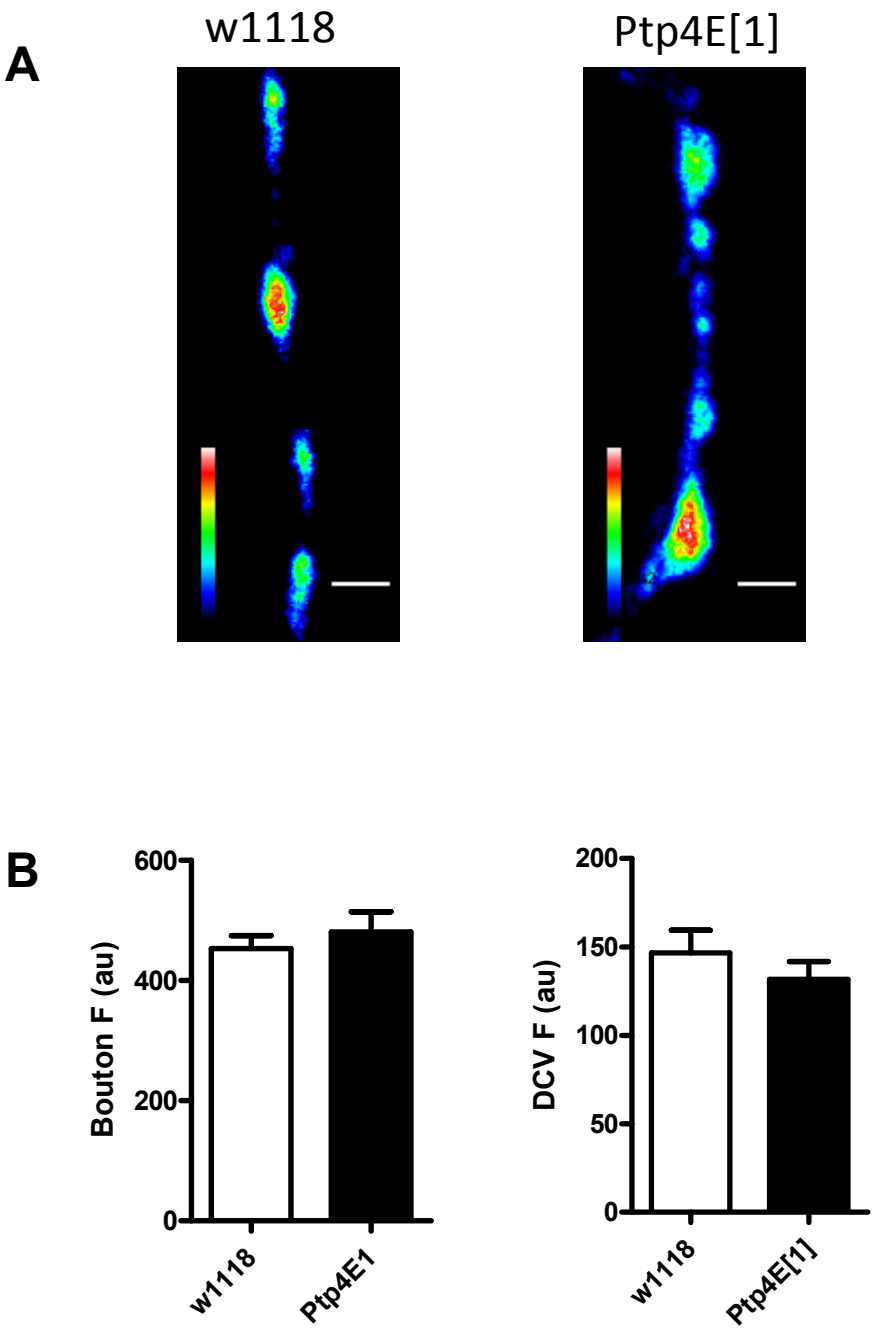

Figure S1. No effect of Ptp4E[1] on type III boutons. A. Pseudo-color images showing similar Dilp2-GFP levels in type III boutons on muscle 12 of control (w1118) and Ptp4E[1] animals. Bar, 2 μm. B. Quantification of fluorescence in boutons and transport DCVs between boutons in control (w1118) and Ptp4E[1] animals. N=15 for each bar.